




Sodium cholate as efficient green reducing agent for graphene oxide via flow reaction for flexible supercapacitor electrodes

Kam Sheng Lau¹ · Riski Titian Ginting² · Sin Tee Tan³ · Siew Xian Chin⁴ · Sarani Zakaria¹ · Chin Hua Chia¹ 

Received: 22 February 2019 / Accepted: 24 September 2019
© Springer Science+Business Media, LLC, part of Springer Nature 2019

Abstract

In this work, sodium cholate (NaC) was used as novel green reducing agent for graphene oxide (GO) reduction at 90 °C and short synthesis time using a continuous segmented flow reaction system. As a comparison, we had used the common reducing agent which is glucose to study its chemical and electrochemical properties. The morphologies of GO and reduced-graphene oxide (rGO) were characterized with X-ray photoelectron spectroscopy (XPS), field emission scanning electron microscope (FESEM), Fourier transformed infrared (FTIR), Raman and Ultraviolet–Visible (UV–Vis) spectroscopy analysis demonstrated that reduction of GO occurred. For electrochemical measurements, the rGO was cast on carbon cloth to investigate the electrochemical performance with cyclic voltammetry (CV) and galvanostatic charge–discharge (GCD) measurements. NaC assisted rGO (rGO–NaC) was able to achieve a specific capacitance up to 94 F g^{−1} at 0.1 A g^{−1} and remarkable capacitance retention of 103% after 10,000 cycles. A flexible test shows that rGO–NaC bendable at 0°–60°. These results demonstrate that rGO–NaC is promising as flexible supercapacitors electrodes.

1 Introduction

Two-dimensional (2D) carbon-based materials such as graphene, graphene oxide (GO), and reduced graphene oxide (rGO) have been used for various of applications, such as electronics, sensors, separations, and coatings, due to their distinctive structures and properties [1, 2]. Chemical reduction of GO using hydrazine, which is the most efficient reductant, however hydrazine is highly toxic and carcinogenic [3, 4]. Besides, the stability of rGO which more favorable in polar protic solvents limits in large-scale and

sustainable productions [5, 6]. Therefore, replacing it with greener reductant which stable in universal solvent is crucial for a sustainable synthesis of rGO. For the ease of production of rGO, we had adapted flow synthesis method which has advantages such as effective heat transfer, faster and safer reaction, easy scale-up and continuous process [7, 8].

rGO has been proposed in supercapacitor applications and characterized in term electrochemical performance due to the presence of remaining oxygenated functional groups and structural defects [9, 10]. However, the theoretical capacitance of 550 F g^{−1} of graphene has not been achieved which draws the attention of this research [11]. Besides, there are some other types of capacitive materials, such as hexaferrites, metal oxides, conductive polymers, etc. [12–15]. Furthermore, hydrazine-reduced-GO coated on nickel foam was proven able to achieve capacitance of 166.8 mF cm^{−3} at scan rate of 10 mV s^{−1} in 5 M lithium chloride electrolyte solution [16]. Gong et al. synthesized hydrothermally reduced GO, and its specific capacitance was 67.9 F/g [17]. Graphene synthesis via chemical vapor deposition method using methane gas on nickel foam was studied by Chen et al., and a specific capacitance of 55.3 F g^{−1} was obtained using 1 M sodium acetate and 1 M magnesium sulfate as electrolyte [18].

Generally, NaC was commonly used as a stabilizer for graphene dispersion [19]. However, we found that

✉ Riski Titian Ginting
titiangt@unprimdn.ac.id

✉ Chin Hua Chia
chia@ukm.edu.my

¹ Materials Science Program, Faculty of Science and Technology, Universiti Kebangsaan Malaysia, 43600 Bangi, Selangor, Malaysia

² Department of Electrical Engineering, Universitas Prima Indonesia, Medan 20118, Indonesia

³ Department of Physics, Faculty of Science, Universiti Putra Malaysia, 43400 UPM Serdang, Selangor, Malaysia

⁴ ASASipintar Program, Pusat GENIUS@Pintar Negara, Universiti Kebangsaan Malaysia, 43600 Bangi, Selangor, Malaysia

NaC demonstrates better reduction due to the presence of hydroxyl groups on its structure. Herein, the reduction of GO using green reducing agents such as sodium cholate (NaC) synthesized via continuous flow reaction enable to achieve a production rate of 11 mL s^{-1} of 0.1 wt% rGO. Generally, NaC was commonly used as a stabilizer for graphene dispersion [19]. Therefore, in this study, we would like to investigate the efficiency of NaC in the reduction of GO and its application as electrode in supercapacitor.

2 Experimental

2.1 Materials

Graphite flakes (+100 mesh, $\geq 75\%$ min) and D-glucose ($> 99.5\%$, Hybri-Max™) were purchased from Sigma Aldrich. Cholic acid sodium salt ($> 96.0\%$ by TLC), hydrogen peroxide (30%, EMSURE®ISO), potassium permanganate ($> 99\%$, EMSURE®ISO), sulfuric acid (95–97%, EMSURE®ISO) were purchased from Merck Millipore. Fluorinert™ Electronic Liquid FC-70 was purchased from 3 M™. Hydrochloric acid (37%, AR grade) and O-Phosphoric acid (85%, AR grade) were purchased from R&M Chemicals. Carbon cloth ($< 13 \text{ m}\Omega \text{ cm}^2$) was purchased from Ce-tech Co., Ltd.

2.2 Sample preparation

GO was prepared using modified Hummers method [20]. Typically, 3 g of graphite flakes and 18 g KMnO_4 were added into 360 mL of $\text{H}_2\text{SO}_4\text{:H}_3\text{PO}_4$ in 9:1 ratio and stirred for 30 h to undergo oxidation process. After that, the oxidation process was terminated by adding suitable amount of H_2O_2 . The oxidized graphite was centrifuged and washed with diluted HCl and subsequently with deionized water for 5 times each to remove the metal ions and acid. During this step, oxidized graphite was exfoliated and formed a GO gel. The solid content of the produced GO suspension was analyzed with moisture analyzer (AnD, model MX-50) and further diluted to achieve 0.2 wt% GO solution. Reduction of GO was performed using a flow reactor system (Uniqsis Ltd.). First, 0.2 wt% GO solution was mixed with 1 M of NaC solution by stirring for 300 s. The mixture and an immiscible liquid FC-70 (3 M) were injected into separate injection loop and pumped at a flow rate of 0.1 mL min^{-1} to obtain a nominal residence time of 50 min in the reactor coil which was heated at 90°C . The product (rGO–NaC) was collected and washed with deionized water for three times by centrifugation. Similar procedure was repeated using 1 M of glucose as a comparison. The product was denoted as rGO–Glu.

2.3 Characterization

The morphology of the samples were examined by a field emission scanning electron microscope (FESEM, Zeiss Merlin) and Fourier transformed infrared (FTIR) spectra were recorded using a FTIR spectrometer (Bruker, Alpha). The samples were investigated by a Raman micro-spectroscopy (uRaman-Ci, Technospex) equipped with a 532 nm laser and an optical microscope (Nikon Eclipse Ci L), where the exposure power and time of the laser are 0.5 mW and 5 s. The Ultraviolet–Visible (UV–Vis) spectra were obtained using a UV–Vis spectrophotometer (Jenway 7315). The C 1s spectrum was obtained by using Auger Electron Spectroscopy with X-Ray photoelectron spectrometer (AES-XPS, Kratos).

2.4 Electrochemical analyses

The electrochemical behavior of the samples was measured with a three-electrode system using 1 M H_3PO_4 as the electrolyte, a Ag/AgCl (3 M KCl, CHI-Instruments) electrode as the reference electrode and a platinum wire as counter electrode. For the working electrode, rGO–NaC and rGO–Glu solutions were cast on cleaned carbon cloth (CC) with controlled mass loading of 1.5 mg cm^{-2} , followed by drying at 70°C for 0.5 h and labeled as CC/rGO–Glu and CC/rGO–NaC. Cyclic voltammetry (CV) and Galvanostatic Charge–Discharge (GCD) measurements were measured using Gamry Instrument (Reference 600). The specific capacitance of the sample was calculated based on the area under the GCD analysis using the equation shown as below:

$$\text{Specific capacitance}(C_{\text{sp}}) = \frac{I \times t}{m \times \Delta V} \quad (1)$$

where I , t , ΔV is charging current, discharge time, mass loading, and discharging potential window, respectively. A flexibility measurement was conducted by pinching bend the sample for 10 min at different angles before measuring its C_{sp} using CV curves at 50 mV s^{-1} .

3 Results and discussion

The morphologies of pristine GO, rGO–NaC and rGO–Glu are shown in Fig. 1a–c. The morphology of GO changed upon reduction, as agglomeration of individual rGO sheets occurred and formed a thicker sheet layer. Figure 2 shows the FTIR spectra of the GO and rGO samples. The bands at 2919 and 2847, 1720, 1625, 1367, 1254, and 1075 cm^{-1} are corresponding to the stretching modes of C–H, C=O, C=C, C–H, C–O for ether groups, and C–O bond for primary alcohol groups, respectively, in accordance to the previous

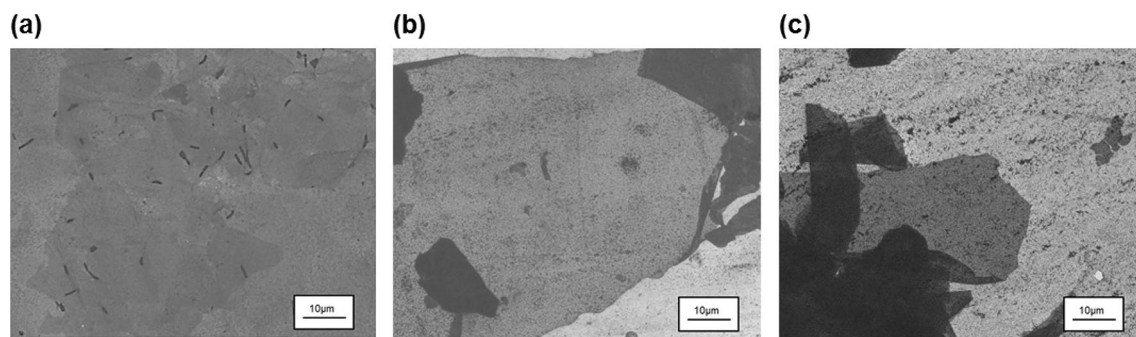


Fig. 1 FESEM images of **a** GO, **b** rGO-Glu, and **c** rGO-NaC

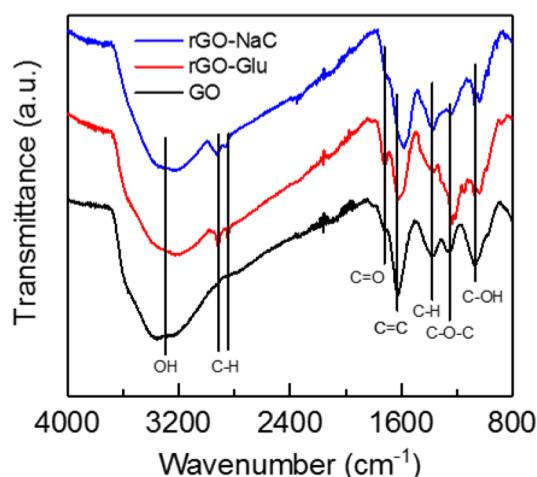


Fig. 2 FTIR spectra for GO, rGO-Glu and rGO-NaC

finding [21]. The observation for the presence of broad peak in spectra for the samples which represents the –OH stretching vibration were due to the absorption of water molecules on the sample surface. After reduction using glucose and NaC, new peaks appeared around 2915 and 2845 cm^{-1} which indicate the presence of C–H bonding mainly from sp^3 hybridized carbons and aldehyde groups [22]. The wavenumber around 1625 cm^{-1} which represent the C=C bond had slightly shifted to lower wavenumber, suggesting the increase of bond length. Interestingly, rGO-Glu and rGO-NaC demonstrate an absorption peak at 1036 cm^{-1} , suggesting the reduction –COOH and –CHO groups of GO into primary alcohol –C–OH group.

The Raman shifts of the GO and rGO are elucidated in Fig. 3 to characterize the order or disorder degree of carbon materials, i.e., the higher I_D/I_G , the larger disorder degree of the carbon materials [23]. There were two significant peaks which are D and G bands, representing the breathing mode of κ -point phonons of A_{1g} symmetry of out-of-plane structural defects and first-order scattering of the E_{2g} phonon in graphitic material within sp^2 bonded

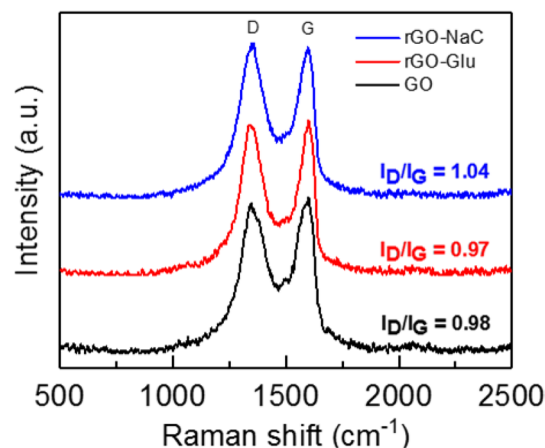


Fig. 3 Raman spectra for GO, rGO-Glu and rGO-NaC

carbon atoms, respectively [24, 25]. The D and G peaks located at 1348 and 1600 cm^{-1} show typical Raman features of disordered graphene with slight increase of I_D/I_G ratio for rGO-NaC compared to pristine GO and rGO-Glu, which can be ascribed to the removal of the oxygenated functional groups upon reduction, leading to the decrease in average size of the sp^2 domain and increased fraction of graphene edges, thus increasing the defects [26]. Besides, the FWHM of G peaks of GO (83.3) decreases to 56.0 and 57.7 after reduction process using Glu and NaC, respectively, which are consistency with the I_D/I_G values.

Figure 4 shows the absorption spectra of GO and rGO reduced by using various reducing agents. As we can observe, the GO sample shows two characteristics peaks at 230 nm and 272 nm, which are corresponding to aromatic C=C bonds $\pi - \pi^*$ transition of and C=O bonds $n - \pi^*$ transition, respectively [27, 28]. After the reduction process, the absorption peak of GO at 230 nm is red-shifted for all the samples and NaC-rGO exhibited the largest shifting to 246 nm among all. The red shifted peak observed suggesting a successive reduction process

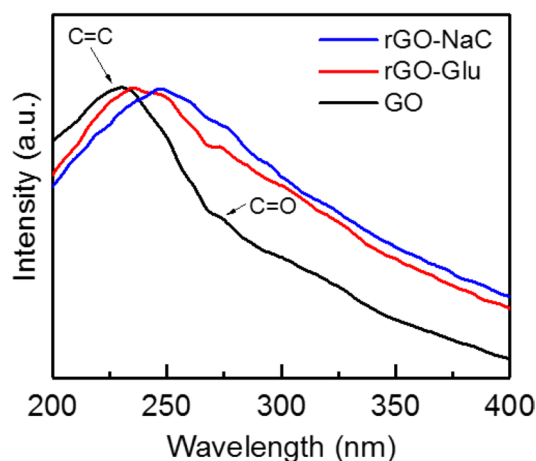


Fig. 4 UV-Vis spectra of GO, rGO-Glu and rGO-NaC

to rGO which cause by the restoration of conjugation of C=C bond on the graphene oxide [29, 30].

We have proposed the oxidation mechanism of NaC and glucose for the reduction of GO as shown in Fig. 5. The functional groups in the NaC structure (Fig. 5a) that have oxidation affinity which is the hydroxyl groups at position 3, 7, and 12. It may undergo oxidation to yield ketone groups [31, 32]. Figure 5b illustrated the oxidation mechanism of glucose to gluconic acid, in which the ketone group on the glucose can be oxidized to carboxylic acid [33, 34]. Concurrently, the reduction process occurred on the carboxylic and ketone groups on the GO, which were reduced to produce rGO.

In order to further understand the chemical states of elements of samples, XPS measurement was performed. Figure 6a, b exhibit the C 1s XPS spectra of GO and rGO-NaC after deconvolution and the peak area was tabulated in Table 1. The peaks specify a considerable degree of

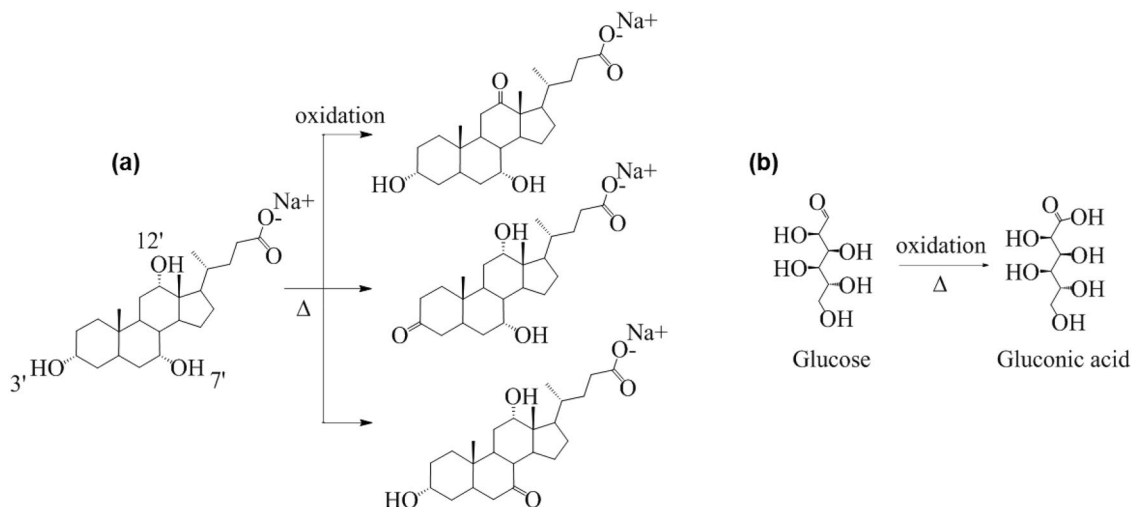


Fig. 5 Proposed mechanism for oxidation of **a** NaC and **b** glucose

Fig. 6 C 1s XPS spectrum of **a** GO and **b** rGO-NaC

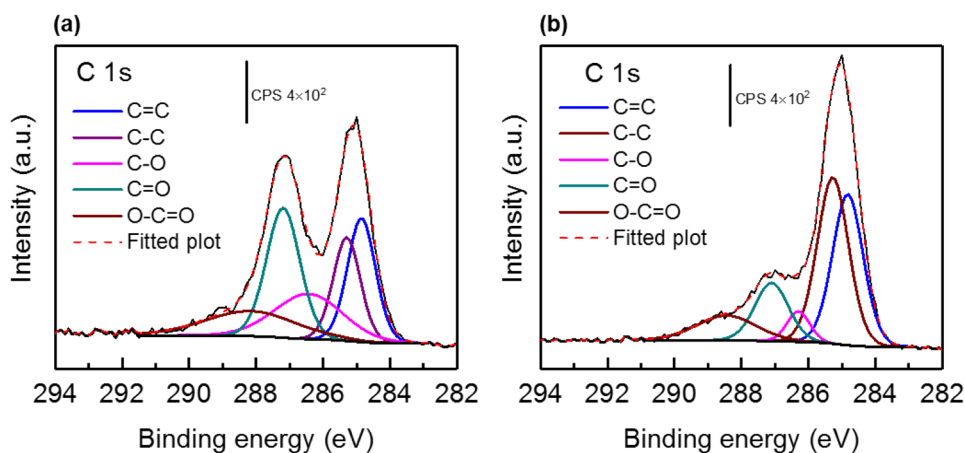


Table 1 The deconvoluted C 1s XPS peak area of GO and rGO–NaC

	C=C (%)	C–C (%)	C–O (%)	C=O (%)	O–C=O (%)
GO	21.72	17.61	19.15	27.16	14.35
rGO–NaC	33.1	37.34	4.95	14.01	10.59

oxidation which corresponds to the carbon atoms in different functional groups located at 284.9, 285.3, 286.5, 287.2, and 288.2 attributed to the C=C, C–C, C–O, C=O, and O–C=O groups, respectively [35–37]. Although upon reduction process, the peaks corresponding to C=C and C–C of rGO–NaC were increased due to the reduction process. However, some remaining C=O and O–C=O can still be observed which could arise from remaining oxygenated functional groups on rGO and NaC that bound on the surface of rGO [38, 39]. The XPS results are in line with the observation of the increase in I_D/I_G in Raman spectra upon restoration of C=C bonds and the presence of sp^3 C–H group in FTIR spectra.

The electrochemical performance of rGO–Glu and NaC coated on CC was measured using three electrode system. Cyclic voltammetry (CV) curves of both CC/rGO–NaC and CC/rGO–Glu demonstrate a quasi-rectangular shape from 0 to 0.8 V at scan rate of 50 mV s^{-1} (see Fig. 7a) indicates good electrical double layer capacitive behavior. Compared to CC/rGO–Glu, CC/rGO–NaC presents a larger integrated

area in the CV curve, implying an enhanced capacitance. In addition, GCD curves show that CC/rGO–NaC has a longer discharge time than CC/rGO–Glu (Fig. 7b). Figure 7c, d depict the GCD curves at various current densities for CC/rGO–Glu and CC/rGO–NaC, respectively, and nearly triangular shape without obvious voltage decline, revealing the low internal resistance of the sample. Moreover, the calculated C_{sp} increases from 10 to 93 F g^{-1} at 0.1 A g^{-1} and from 7 to 56 F g^{-1} at 1 A g^{-1} for CC/rGO–Glu and NaC, respectively, as shown in Fig. 7e, which is consistent with the CV result. The decrease in C_{sp} with increasing current density can be ascribed to the shorter time of ionic diffusion, thus hinder the charge storage on the electrode's surface and hence lowered the capacitance. The improvement of electrochemical performance of CC/rGO–NaC is due to the reduction process of GO to rGO using 1 M of NaC which decreases the average crystallite size of sp^2 domain. As it well known the average crystallite size strongly affects the electrochemical performance, the decrease in crystallite size of sp^2 domain improves the mass transport of H_3PO_4 electrolyte to the rGO, especially oxygen and oxygen vacancies transport. Besides, the destroyed grains of rGO could also decrease its resistivity [40, 41]. Furthermore, the long-term cyclic performance of CC/rGO–NaC was tested by GCD at 1 A g^{-1} .

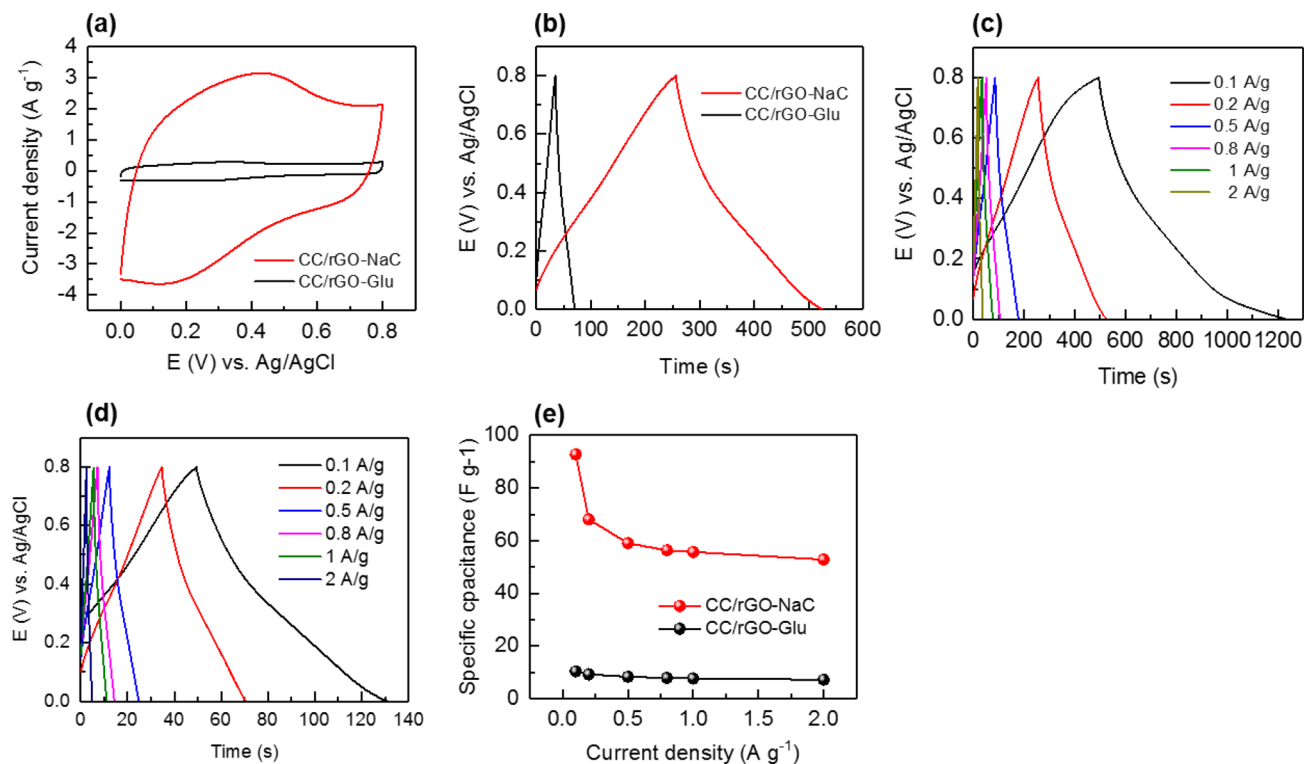
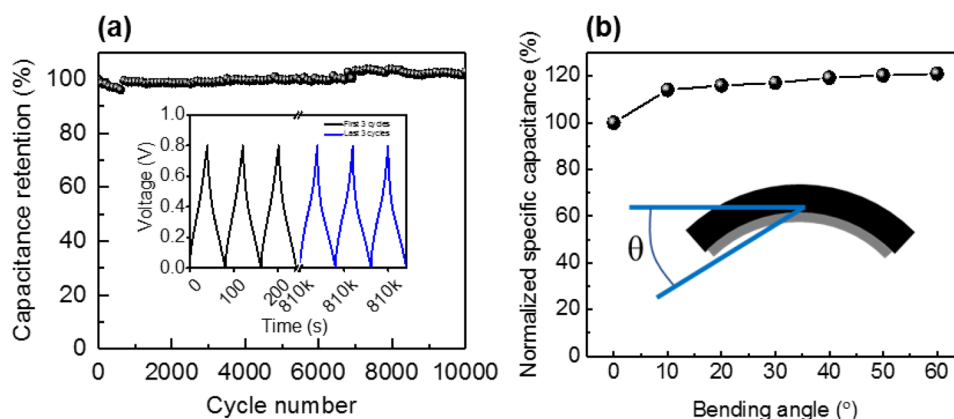


Fig. 7 Comparison for **a** CV at 50 mV s^{-1} and **b** GCD at 0.2 A g^{-1} for CC/rGO–Glu and CC/rGO–NaC. Results for charge–discharge for **c** CC/rGO–NaC **d** CC/rGO–Glu. **e** C_{sp} calculated from discharge time

Fig. 8 **a** Cyclic stability of CC/rGO–NaC at 1 A g^{−1}. Inset shows the first (black line) and last 3 charge–discharge (blue line) cycles. **b** Flexible test. Inset shows the bending angle measured (Color figure online)



The cyclic stability of the CC/rGO–NaC was analyzed with GCD measurement at 1 A g^{−1} for 10,000 cycles as shown in Fig. 8a. The capacitance maintained at 103% of the initial capacitance even after 10,000 cycles due to electrochemical self-activation [42]. In addition, flexibility test (see Fig. 8b) for CC/rGO–NaC was conducted show that CC/rGO–NaC had a slightly increased in C_{sp} after bending at 10–60°. The flexibility measurement concluded that the rGO–NaC is stable and bendable, promising to be used as capacitive material on flexible devices.

4 Conclusion

Continuous flow reduction of GO using NaC as green reducing agent was studied. Successful reduction of GO using NaC was supported by the results obtained from the characterizations which show the increase in defect and reduce in oxygenated functional groups on rGO formed. The CC/rGO–NaC gives the highest C_{sp} of 93 F g^{−1} at 0.1 A g^{−1} and able to maintain capacitance retention of 103% after 10,000 cycles at 1 A g^{−1}. Flexible test for the CC/rGO–NaC electrode shows its potential for flexible supercapacitor device.

Acknowledgements The authors would like to thank the Centre of Research and Instrumentation (CRIM), UKM for the research grants (Grant Nos. GUP-2017-055 & GUP-2018-159) provided.

References

1. K.K.H. De Silva, H.-H. Huang, R.K. Joshi, M. Yoshimura, Chemical reduction of graphene oxide using green reductants. *Carbon* **119**, 190–199 (2017)
2. M.S. Poorali, M.M. Bagheri-Mohagheghi, Comparison of chemical and physical reduction methods to prepare layered graphene by graphene oxide: optimization of the structural properties and tuning of energy band gap. *J. Mater. Sci.: Mater. Electron.* **27**, 260–271 (2016)
3. S. Stankovich, D.A. Dikin, R.D. Piner, K.A. Kohlhaas, A. Kleinhammes, Y. Jia, Y. Wu, S.T. Nguyen, R.S. Ruoff, Synthesis of graphene-based nanosheets via chemical reduction of exfoliated graphite oxide. *Carbon* **45**, 1558–1565 (2007)
4. M.-S. Poorali, M.-M. Bagheri-Mohagheghi, Comparison of chemical and physical reduction methods to prepare layered graphene by graphene oxide: optimization of the structural properties and tuning of energy band gap. *J. Mater. Sci.: Mater. Electron.* **27**, 260–271 (2016)
5. K. Chen, C. Li, L. Shi, T. Gao, X. Song, A. Bachmatiuk, Z. Zou, B. Deng, Q. Ji, D. Ma, H. Peng, Z. Du, M.H. Rummeli, Y. Zhang, Z. Liu, Growing three-dimensional biomorphic graphene powders using naturally abundant diatomite templates towards high solution processability. *Nat. Commun.* **7**, 13440 (2016)
6. K.S. Siow, Pengelupasan grafit untuk mengkomersilkan teknologi grafir. *Sains Malays.* **46**, 1047–1059 (2017)
7. D. Dallinger, C.O. Kappe, Why flow means green—evaluating the merits of continuous processing in the context of sustainability. *Curr. Opin. Green Sustain. Chem.* **7**, 6–12 (2017)
8. F. Zhang, N. Song, S. Zhang, S. Zou, S. Zhong, Synthesis of sponge-loaded Bi₂WO₆/ZnFe₂O₄ magnetic photocatalyst and application in continuous flow photocatalytic reactor. *J. Mater. Sci.: Mater. Electron.* **28**, 8197–8205 (2017)
9. Q. Ke, J. Wang, Graphene-based materials for supercapacitor electrodes—a review. *J. Mater.* **2**, 37–54 (2016)
10. E.T. Mombeshora, V.O. Nyamori, Physicochemical characterisation of graphene oxide and reduced graphene oxide composites for electrochemical capacitors. *J. Mater. Sci.: Mater. Electron.* **28**, 18715–18734 (2017)
11. J. Zhu, A.S. Childress, M. Karakaya, S. Dandeliya, A. Srivastava, Y. Lin, A.M. Rao, R. Podila, Defect-engineered graphene for high-energy- and high-power-density supercapacitor devices. *Adv. Mater.* **28**, 7185–7192 (2016)
12. V.A. Turchenko, S.V. Trukhanov, A.M. Balagurov, V.G. Kostishyn, A.V. Trukhanov, L.V. Panina, E.L. Trukhanova, Features of crystal structure and dual ferroic properties of BaFe₁₂-xMxO₁₉ (Me = In³⁺ and Ga³⁺; x = 0.1–1.2). *J. Magn. Magn. Mater.* **464**, 139–147 (2018)
13. S.V. Trukhanov, A.V. Trukhanov, V.A. Turchenko, A.V. Trukhanov, D.I. Tishkevich, E.L. Trukhanova, T.I. Zubar, D.V. Karpinsky, V.G. Kostishyn, L.V. Panina, D.A. Vinnik, S.A. Gudkova, E.A. Trofimov, P. Thakur, A. Thakur, Y. Yang, Magnetic and dipole moments in indium doped barium hexaferrites. *J. Magn. Magn. Mater.* **457**, 83–96 (2018)
14. N. Kumar, R.T. Ginting, M. Ovhal, J.-W. Kang, All-solid-state flexible supercapacitor based on spray-printed polyester/PEDOT:PSS electrodes. *Mol. Cryst. Liq. Cryst.* **660**, 135–142 (2018)

15. W.H. Low, P.S. Khiew, S.S. Lim, C.W. Siong, E.R. Ezeigwe, Recent development of mixed transition metal oxide and graphene/mixed transition metal oxide based hybrid nanostructures for advanced supercapacitors. *J. Alloys Compd.* **775**, 1324–1356 (2019)
16. F. Wang, Y. Zeng, D. Zheng, C. Li, P. Liu, X. Lu, Y. Tong, Three-dimensional iron oxyhydroxide/reduced graphene oxide composites as advanced electrode for electrochemical energy storage. *Carbon* **103**, 56–62 (2016)
17. Y. Gong, D. Li, Q. Fu, C. Pan, Influence of graphene microstructures on electrochemical performance for supercapacitors. *Prog. Nat. Sci. Mater. Int.* **25**, 379–385 (2015)
18. W. Chen, Z. Fan, G. Zeng, Z. Lai, Layer-dependent supercapacitance of graphene films grown by chemical vapor deposition on nickel foam. *J. Power Sources* **225**, 251–256 (2013)
19. S. De, P.J. King, M. Lotya, A. O'Neill, E.M. Doherty, Y. Hernandez, G.S. Duesberg, J.N. Coleman, Flexible, transparent, conducting films of randomly stacked graphene from surfactant-stabilized, oxide-free graphene dispersions. *Small* **6**, 458–464 (2010)
20. N.M. Huang, H.N. Lim, C.H. Chia, M.A. Yarmo, M.R. Muhamad, Simple room-temperature preparation of high-yield large-area graphene oxide. *Int. J. Nanomed.* **6**, 3443–3448 (2011)
21. S. Sadhukhan, T.K. Ghosh, D. Rana, I. Roy, A. Bhattacharyya, G. Sarkar, M. Chakraborty, D. Chattopadhyay, Studies on synthesis of reduced graphene oxide (RGO) via green route and its electrical property. *Mater. Res. Bull.* **79**, 41–51 (2016)
22. G. Marami, S.A. Nazari, S.A. Faghidian, F. Vakili-Tahami, S. Etemadi, Improving the mechanical behavior of the adhesively bonded joints using RGO additive. *Int. J. Adhes. Adhes.* **70**, 277–286 (2016)
23. H.-W. Tien, Y.-L. Huang, S.-Y. Yang, J.-Y. Wang, C.-C.M. Ma, The production of graphene nanosheets decorated with silver nanoparticles for use in transparent, conductive films. *Carbon* **49**, 1550–1560 (2011)
24. D. Yang, A. Velamakanni, G. Bozoklu, S. Park, M. Stoller, R.D. Piner, S. Stankovich, I. Jung, D.A. Field, C.A. Ventrice, R.S. Ruoff, Chemical analysis of graphene oxide films after heat and chemical treatments by X-ray photoelectron and Micro-Raman spectroscopy. *Carbon* **47**, 145–152 (2009)
25. A. Ferrari, J. Robertson, Interpretation of Raman spectra of disordered and amorphous carbon. *Phys. Rev. B* **61**, 14095–14107 (2000)
26. Z. Bo, X. Shuai, S. Mao, H. Yang, J. Qian, J. Chen, J. Yan, K. Cen, Green preparation of reduced graphene oxide for sensing and energy storage applications. *Sci. Rep.* **4**, 4684 (2014)
27. I. Roy, D. Rana, G. Sarkar, A. Bhattacharyya, N.R. Saha, S. Mondal, S. Pattanayak, S. Chattopadhyay, D. Chattopadhyay, Physical and electrochemical characterization of reduced graphene oxide/silver nanocomposites synthesized by adopting a green approach. *RSC Adv.* **5**, 25357–25364 (2015)
28. K. Krishnamoorthy, R. Mohan, S.-J. Kim, Graphene oxide as a photocatalytic material. *Appl. Phys. Lett.* **98**, 244101 (2011)
29. J. Zhang, H. Yang, G. Shen, P. Cheng, J. Zhang, S. Guo, Reduction of graphene oxide via l-ascorbic acid. *Chem. Commun.* **46**, 1112–1114 (2010)
30. D. Li, M.B. Müller, S. Gilje, R.B. Kaner, G.G. Wallace, Processable aqueous dispersions of graphene nanosheets. *Nat. Nanotechnol.* **3**, 101–105 (2008)
31. P.S. Dangate, C.L. Salunke, K.G. Akamanchi, Regioselective oxidation of cholic acid and its 7β epimer by using o-iodoxybenzoic acid. *Steroids* **76**, 1397–1399 (2011)
32. H. Kimura, A. Okamura, H. Kawaide, Oxidation of 3-, 7-, and 12-hydroxyl groups of cholic acid by an alkalophilic bacillus sp. *Biosci. Biotechnol. Biochem.* **58**, 1002–1006 (1994)
33. O. Akhavan, E. Ghaderi, S. Aghayee, Y. Fereydooni, A. Talebi, The use of a glucose-reduced graphene oxide suspension for photothermal cancer therapy. *J. Mater. Chem.* **22**, 13773 (2012)
34. C. Xu, X. Shi, A. Ji, L. Shi, C. Zhou, Y. Cui, Fabrication and characteristics of reduced graphene oxide produced with different green reductants. *PLoS ONE* **10**, e0144842 (2015)
35. K. Zangeneh Kamali, A. Moradi Golsheikh, Green and facile approach to synthesis of well-dispersed nitrogen-doped graphene without using surfactant or stabilizer with potential application for oxygen reduction reaction. *Colloids Surf. A* **509**, 574–582 (2016)
36. Y. Zhou, D. Li, L. Yang, C. Li, Y. Liu, J. Lu, Y. Wang, Preparation of 3D urchin-like RGO/ZnO and its photocatalytic activity. *J. Mater. Sci.: Mater. Electron.* **28**, 7935–7942 (2017)
37. K.K.H. De Silva, H.H. Huang, M. Yoshimura, Progress of reduction of graphene oxide by ascorbic acid. *Appl. Surf. Sci.* **447**, 338–346 (2018)
38. C. Li, Z. Zhuang, X. Jin, Z. Chen, A facile and green preparation of reduced graphene oxide using Eucalyptus leaf extract. *Appl. Surf. Sci.* **422**, 469–474 (2017)
39. T. Wang, J. Lin, Z. Chen, M. Megharaj, R. Naidu, Green synthesized iron nanoparticles by green tea and eucalyptus leaves extracts used for removal of nitrate in aqueous solution. *J. Clean. Prod.* **83**, 413–419 (2014)
40. S.V. Trukhanov, A.V. Trukhanov, C.E. Botez, A.H. Adair, H. Szymczak, R. Szymczak, Phase separation and size effects in $\text{Pr}_{0.70}\text{Ba}_{0.30}\text{MnO}_{3+\delta}$ perovskite manganites. *J. Phys.: Condens. Matter* **19**, 266214 (2007)
41. S.V. Trukhanov, Investigation of stability of ordered manganites. *J. Exp. Theor. Phys.* **101**, 513–520 (2005)
42. F. Ran, X. Zhang, Y. Liu, K. Shen, X. Niu, Y. Tan, L. Kong, L. Kang, C. Xu, S. Chen, Super long-life supercapacitor electrode materials based on hierarchical porous hollow carbon microcapsules. *RSC Adv.* **5**, 87077–87083 (2015)

Publisher's Note Springer Nature remains neutral with regard to jurisdictional claims in published maps and institutional affiliations.